Optica Applicata, Vol. XLIII, No. 4, 2013
DOI: 10.5277/oa130411

Determination of the optode array representation using optical properties at systole and diastole

NUR ANIDA JUMADI[1, 2*], GAN KOK BENG[3], MOHD ALAUDDIN MOHD ALI[2], EDMOND ZAHEDI[2]

[1]Department of Electronics Engineering, UTHM, Batu Pahat, Malaysia

[2]Department of Electrical, Electronics and System, UKM, Bangi, Malaysia

[3]Institute of Space Science, UKM, Bangi, Malaysia

[*]Corresponding author: anida@uthm.edu.my

The necessity to develop an optode array in order to probe the fetus oxygenation noninvasively regardless of the fetus position has been highlighted in previous literature. In this paper, a series of optical simulations are carried out to determine the best representation of optode array by using optical properties at systolic and diastolic states. The selection is based on the highest flux values accumulated at respective detectors. To accomplish the objective, a homogenous three-layer semi-infinite tissue model is implemented to represent the pregnant woman model. The geometry of the model as well as Monte Carlo simulation are carried out using commercial software, whereas the optical properties related to systolic and diastolic states are defined for all wavelengths. A statistical noise analysis is also introduced in order to find a sufficient number of rays to be launched into the optical tissue system.

Keywords: optical simulation, optical properties, optode array, semi-infinite tissue layer, statistical analysis.

1. Introduction

Fetal surveillance monitoring is crucial as it helps to avoid fetal hypoxia or intrapartum asphyxia that can bring damage to the vital organs such as heart and brain and this can be done by detecting a decrease in oxygen supply in fetus. In conjunction with the use of cardiotocography (CTG), a fetal scalp blood sampling (FBS) technique has been used to determine hypoxia in fetus with an abnormal heart rate pattern by measuring the pH or lactate. Intervention will be recommended if the pH reading shows less than 7.24 or when abnormal lactate points at 4.20 or higher [1].

Although this method can assist medical practitioners or midwifes to handle fetal distress during labor or near labor, it has several limitations. First of all, the FBS method is an invasive procedure, non-continuous, technically uneasy and difficult to obtain an adequate blood sample [2, 3]. Secondly, it shows high failure in sampling and

analysis of pH blood at the range of 10.4 to 25% and consumes time in collecting or analysing the data; thus increasing the delay in clinical management [4–6].

The fetal oximetry system is initially developed purposely for intrapartum monitoring [7, 8]. It is reported that continued monitoring of fetal oxygen saturation combined with fetal heart rate monitoring may improve accuracy in the evaluation of fetal well-being [9]. Moreover, it is also recommended to monitor the fetal status using intrapartum fetal pulse oximetry in cases of non-reassuring or pathological cardiotocography to avoid imminent fetal hypoxia [10]. However, commercial optical sensors for fetal oximetry have several downsides. Firstly, the technique is invasive to mothers. In real clinical situation, the reflectance optical sensors are attached on the fetus scalp or cheek by inserting it through the birth canal [11]. Besides that, it is reported that the sensors may leave marks on the skin of the fetus [12] and also contribute to the increased number of caesarean sections for dystocia due to the presence of the sensors itself [13].

To overcome those limitations, a transabdominal measuring of fetus oxygen saturation has been presented by [8, 14–20]. The feasibility of transabdominal oximetry was studied from various aspects, starting from the modelling of photon migration through the fetal head until the development of clinical and experimental models by using continuous wave near infrared spectroscopy [8, 14, 15]. Despite the tremendous works mentioned above, only VINTZILEOS *et al*. [20] claimed to be the first who successfully measured the fetal oxygen saturation values on maternal abdomen with the reported value of fetus oxygen saturation between 54 and 74%.

The idea of using a low-cost near-infrared (NIR) light emitting diode (LED) and a silicon photodetector to detect the fetal heart rate (FHR) transabdominally has been proposed by [21]. To obtain the clinical trial results of FHR, the fetal position needs to be determined first by using the CTG and the results revealed that the fetal position affects the accuracy of the FHR with the best results attained when the probe is close to fetal tissues. The promising results have led to another possibility of exploring the noninvasive fetus oxygen saturation measurement by using a low-cost light source instead of using spectroscopy. In addition to that, all previous works mentioned before have not yet explored the optode arrays in order to probe the fetal signals independently of fetal position.

The gaps shown here motivate the authors to conduct a study to determine the best configuration of a reflectance optode array by measuring the flux values at respective detectors. Since the oxygen saturation is much dependent on pulsatility of an arterial and nonpulsatility of bloodless tissues, it is worth to investigate how the systolic and diastolic conditions may affect the optode configuration.

2. Optical properties

Optical properties of tissues are usually characterized by three parameters which are the scattering coefficient μ_s, absorption coefficient μ_a and scattering anisotropy fac-

tor g. The anisotropy factor or cosine scatter g represents the amount of light scattered either in forward or backward direction after a scattering event. The scattering and absorption coefficients are proportional to the scattering and absorption cross-sections σ, density of scatterers and absorbers in the medium ρ, and they can be written as:

$$\mu_a = \rho_a \sigma_a \tag{1}$$

$$\mu_s = \rho_s \sigma_s \tag{2}$$

To create the scattering model, four parameters are needed which are: the absorption coefficient μ_a, reduced scattering μ_s', refractive index of tissue n, and scattering phase function. The reduced scattering μ_s' is used to describe the photons diffusion in a random walk after experiencing several scattering events and it is denoted as:

$$\mu_s' = \mu_s(1 - g) \tag{3}$$

The scattering phase function is used to define the new photon direction after each scattering event. As stated by [22], a very general phase function can be applied if the optode spacing is more than 20 mm. In this study, a volumetric scattering phase function is used to guide a new photon direction. A Monte Carlo framework, namely the Advanced System Analysis Program (ASAP), has been used to generate light distribution in the tissue.

In ASAP, the Monte Carlo code is based on the surface. In other words, each surface has a specific type of boundary with the flux dependent on the amount of reflection and transmission as defined at the boundary [23]. The advantages of using this programme are as follows: it gives a 3D simulation of light behavior and takes into account Fresnel reflection and refraction at tissue boundaries.

In a real condition, the lights collected on the detector are modulated with the oxygenated and deoxygenated blood. During systole, more blood is pumped in the arteries and as a result, the absorbance of light is increased; thus the light being

T a b l e 1. Optical properties at two different wavelengths.

	Parameters		
	Coefficient s	Wavelength	
State	[mm^{-1}]	735 nm	890 nm
Systolic	$\Sigma\mu_{a,\,sys,\,m}$	0.01163	0.01473
	$\Sigma\mu_{a,\,sys,\,f}$	0.01261	0.01411
Diastolic	$\Sigma\mu_{a,\,dias,\,m}$	0.01147	0.01435
	$\Sigma\mu_{a,dias,f}$	0.01241	0.01377
	$\mu_s^{t\prime}$	1.22	0.89
	$\Sigma\mu_s'$	1.227	0.895
Amniotic fluid	$\mu_{a,\,af}$	0.00287	0.00359
	$\mu_{s,\,af}'$	0.01	0.01

transmitted is minimal. In contrast to systole, the transmitted light is maximal during diastole due to the minimum absorption of light detected that is caused by the minimum arterial vessel diameter. In order to take the systolic and diastolic conditions into consideration, the optical properties associated with this condition are already defined in the Appendix section and the corresponding values are tabulated in Tab. 1.

All values specified in Tab. 1 are taken from References [24] and [25]. These optical properties represent the oxygen saturation of fetus and maternal at 70% and 90%, respectively. The value of anisotropy factor g associated with mother and fetus is the same: 0.80, whereas for amniotic fluid it is 0.85, and it applies to all wavelengths. On the other hand, the reduced scattering coefficient is wavelength dependent and is assumed to be the same for mother and fetus layers.

3. Model geometry definition

Based on the standard rotational axis which comprises x, y and z axes, the pregnant woman model is structured in three layers as illustrated in Fig. 1 and is assumed as a cylindrical semi-infinite tissue model to resemble a realistic condition. As previously suggested by researchers [26, 27], a three-layer model is reasonable in light of available empirical data. As shown in Fig. 1, the first (yellow), second (blue) and third (green) layers are the mother layer followed by the amniotic fluid layer and fetal layer, respectively.

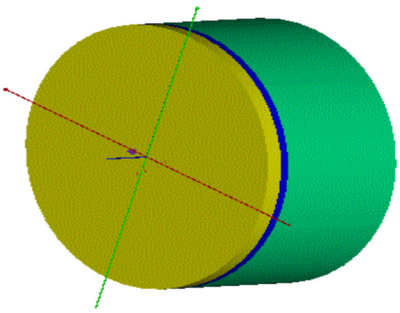

Fig. 1. The geometry model is defined by a 3-layer tissue which comprises (from left) mother, amniotic fluid and fetus.

The length of the fetal layer is set to 200 mm along the z-axis. BEARDEN *et al*. stated that the thickness of the maternal abdominal wall is in the range of 20 to 50 mm [28]. In other study [29], the average abdominal wall thickness measured on 243 pregnant patients (gestation weeks: 26±7) is 24±8 mm, whereas the thickness of the amniotic fluid layer is found to be 13±4 mm. The maternal abdominal thickness used in this simulation is from the latter study. The value for amniotic fluid thickness is taken from the amniotic fluid index. This is the only method available to measure the amniotic fluid thickness and for that reason it can be accepted when modelling the amniotic

fluid layer [24]. To simplify, the typical thickness values for mother and amniotic fluid are being used in this study.

4. Modelling light sources and detectors

A study on how deep is the penetration of light in the tissue is excluded in this paper since the extensive research has been carried out previously [8, 17, 28, 30]. However, their relative merits will be discussed briefly in this section. Previous works, for instance RAMANUJAM *et al*. [8, 14] and GAN *et al*. [21, 24], have shown that longer wavelength penetrates tissue more effectively. Meanwhile, BEARDEN *et al*. [28] suggested that for visible light to penetrate the biological tissue with thickness more than 40 mm, the optimal wavelength should be in the range of 600 to 700 nm.

In the case of noninvasive fetal pulse oximetry, previous researches such as MAWN *et al*. [18] and VINTZILEOS *et al*. [20] utilize 735, 805 and 850 nm as a source of light. This selection of wavelengths is upon the basis of MANNHEIMER *et al*. [25] and ZOURABIAN *et al*. [16] studies. In the latter study, an analysis of optimal wavelength for fetal pulse oximetry based on hemoglobin, water absorption and scattering effects is presented. The results stated that the minimum error in saturation occurred in the range of 670 to 720 nm and 825 to 925 nm in the region of visible light and infrared light, respectively, whereas in the former study, three sets of wavelength pairs had been proposed and the findings show that 660/890 nm and 735/890 nm allow optimum performance during high and low saturation, respectively. On the other hand, although 800/950 pair provides good reading in low saturation, the measurement sensitivity becomes smaller [25].

The type of a light source intended to be modelled in this paper is a light emitting diode (LED). The light source or emitter is created as an incoherent source by modifying the ray flux to match the graphical intensity distribution provided by the LED manufacturer. This process is also known as ray apodization. Although wavelengths related to the minimum error in saturation should be accounted, this error is only significant at smaller optode distance and applied to one wavelength only. Moreover, the ratio of two wavelengths will reduce this error significantly [16]. In addition to that, the lack of information on optical properties of the tissues at these wavelengths caused that only two wavelengths were considered here, that is 735 and 890 nm.

As shown in Fig. 2**a**, a diamond configuration of optode array is being proposed here. The name is given based on the perimeters of the detectors' arrangement. The initial distance between each detector with respect to the source is set at 40 mm. Such distance is chosen because 70% of received optical power contributed from the fetal layer occurred at 40 mm [24].

Square configuration is another option which has also been tested in the simulation. As can be seen in Fig. 2**b**, four detectors are added and labeled starting from D5 until D8; with the distance of 40 mm with respect to the adjacent detectors. All detectors

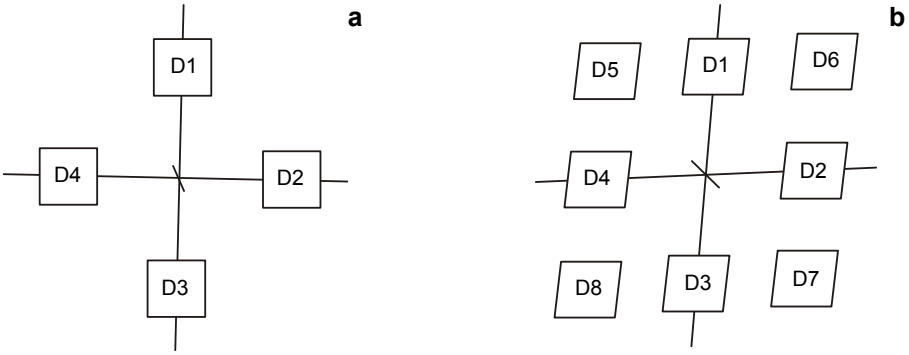

Fig. 2. Detectors arrangement in diamond configuration (**a**) and square configuration (**b**). The position of a light source is at the centre of the origin (0, 0, 0).

are assigned to absorb the light and are modelled as a square with dimension of 10×10 mm^2. This dimension is the actual active area of a photodiode N57-513 (Edmund Optics).

A huge number of rays are required to accurately predict the performance of the optical system. For that reason, a statistical noise is being calculated to determine the sufficient number of rays required for running the simulation. Different number of seeds needs to be applied at selected wavelength and the resulted total flux of all detectors has to be averaged before a standard deviation can be found. In this study, we run for 10th trials and assume that more rays are needed if the standard deviation is more than 1%.

Once the number of rays has been determined, the simulation begins by launching a 735 nm towards the tissue layers that have the optical parameters at a systolic state. In the same way, another simulation is carried out using diastolic parameters.

5. Results and discussion

5.1. Optical simulation

Of three layers, only the amniotic fluid layer is not affected by the systolic and diastolic condition since it has no blood capillaries. Thus, the optical properties at systolic and diastolic states as described in Appendix are for mother and fetus layers. Total flux injected through the model is 1 mW and the propagation of each ray flux is terminated if the power of scattered rays reaches 1.25 pW. A much lower value can be set; however, it will not contribute to the absorption of flux by the detectors. The same number of seed is applied to all simulations for strict reproducibility of the research results.

Monte Carlo modelling is known for the replicability issues when applying different seed numbers [31]. An observation has been made regarding this matter by repeating the same simulation on diamond configuration with different seed number using 735 nm at systolic condition for 10 times at 1 and 5 millions of rays. As expected,

T a b l e 2. Standard deviation calculated using different seed number.

Number of rays	Standard deviation σ	Execution time
1 million	0.005%	19–30 min
5 million	0.002%	120–125 min

the flux values obtained from these simulations are varying depending on the seed numbers due to the stochastic nature of the Monte Carlo process. Considering the variation in optical power associated with the seed number, an analysis in statistical noise has been conducted to find the mean and standard deviation of the optical power for each 10th trial. Using Intel® Core™ 2 Duo, with the speed of 2 GHz and 2 GB RAM computer, the execution time ranges from 19 min to 30 min for 1 million rays, whereas using 5 million rays, the simulation time increased four-fold. Since the standard deviations for both numbers of rays are less than 1%, 1 million of rays are sufficient enough to run the simulation. The details for this finding are presented in Table 2.

5.2. Radiation pattern of light source

Figure 3 shows the resulting ray apodization for 890 nm. The 735 nm are simulated using the same specification as 890 nm. It is quite difficult to obtain the relevant LED datasheets for 735 nm unless the source of light is coming from spectroscopy or laser.

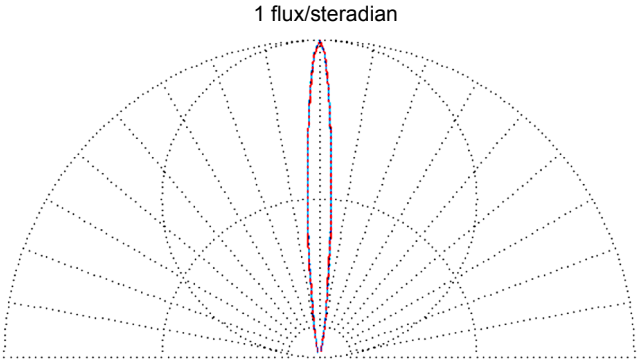

Fig. 3. Simulation of radiation pattern with viewing angle of 36° at 890 nm.

That is why the specification of 890 nm is applied to other wavelengths. By doing this, any disparity in light distribution due to the variation in viewing angle could also be neglected.

5.3. Optical power at detectors

Tables 3 and 4 show the resulting flux collected by detectors in square and diamond configurations, respectively. Looking comparatively at both tables, high flux values

T a b l e 3. Flux values associated with systolic and diastolic states using square configuration.

	Optical power [W]			
	Wavelength 735 nm		Wavelength 890 nm	
Detector	Systolic	Diastolic	Systolic	Diastolic
D1	0.7158×10^{-4}	0.7822×10^{-4}	0.7782×10^{-4}	0.7754×10^{-4}
D2	0.7342×10^{-4}	0.7149×10^{-4}	0.7890×10^{-4}	0.8070×10^{-4}
D3	0.6992×10^{-4}	0.7610×10^{-4}	0.7558×10^{-4}	0.7554×10^{-4}
D4	0.6854×10^{-4}	0.7620×10^{-4}	0.7691×10^{-4}	0.8422×10^{-4}
D5	0.3875×10^{-4}	0.3700×10^{-4}	0.3876×10^{-4}	0.4121×10^{-4}
D6	0.3758×10^{-4}	0.3572×10^{-4}	0.3666×10^{-4}	0.3939×10^{-4}
D7	0.3414×10^{-4}	0.3584×10^{-4}	0.4152×10^{-4}	0.3914×10^{-4}
D8	0.3594×10^{-4}	0.3489×10^{-4}	0.3946×10^{-4}	0.4204×10^{-4}

T a b l e 4. Flux values associated with systolic and diastolic states using diamond configuration.

	Optical power [W]			
	Wavelength 735 nm		Wavelength 890 nm	
Detector	Systolic	Diastolic	Systolic	Diastolic
D1	0.7158×10^{-4}	0.7822×10^{-4}	0.7782×10^{-4}	0.7754×10^{-4}
D2	0.7342×10^{-4}	0.7149×10^{-4}	0.7890×10^{-4}	0.8070×10^{-4}
D3	0.6992×10^{-4}	0.7610×10^{-4}	0.7558×10^{-4}	0.7554×10^{-4}
D4	0.6854×10^{-4}	0.7620×10^{-4}	0.7691×10^{-4}	0.8422×10^{-4}

can be found at D1 to D4 in both configurations, whereas at D5 to D8, the flux values are near or more than 50% less as compared to the first four detectors. These results are not surprising because the more distant the detector is from the source, the less flux will be received by the detector. Also, at D1 to D4, the optical powers during systole and diastole are found to be the same in both configurations due to the same tissue characteristics as well as the number of rays launched into the system.

Besides that, during diastole, the optical power collected at detectors is higher than the flux values at systole condition. This should be expected since physiologically, the absorption of light by hemoglobin is reduced during diastole condition and thus more light can be transmitted through the tissue. However, there are some results that show a contrasting idea by having high flux values during systole. Although this is not fully understood, the main reason is probably due to the stochastic nature of the Monte Carlo simulation process.

Based upon the results and justifications discussed previously, the most suitable optode array that is capable to detect the nearest fetus position is diamond configuration. The finding also suggests the importance to check and compare the SNR (fetal to mother ratio) value at systolic and diastolic states when implementing the optode array probe in the theoretical calibration and future phantom studies. In other words, at any condition, the optical power during diastole should always be higher than at

a systole state. The optical properties employed in this study are based on 90% and 70% blood oxygenation of mother and fetus, respectively. Therefore, using this similar method, a theoretical calibration study can be conducted.

On the other hand, the results obtained probably would differ if any of these parameters changed, *e.g.* when applying different seed number or varying the thickness of each layer. In addition, if the semi-infinite tissue model that has been employed in this work is changed to the physical 3D model of pregnant woman, the values of optical power may differ as well.

5.4. Optical density analysis

Apart from finding the most suitable optode array, another significant feature of obtaining the optical power during systole and diastole is that it enables computation of optical density. In this subsection, an example of how to compute the optical density will be described. The optical density could be calculated by finding the log of the ratio of the light intensity during systole to the light intensity during diastole. In literature [25, 32] an assumption is made that the aforementioned ratio is approximate to the ratio of AC to DC component for small pulse amplitude and hence the same assumption will be applied in this analysis. To simplify, another assumption is made that the flux values collected by detectors are coming from the fetal layer alone. In real case, those flux values contain a mix signal of mother and fetal.

T a b l e 5. The calculated optical density (OD) and OD ratio correspond to the first four detectors.

	Optical density (OD)		
Detector	Wavelength 735 nm	Wavelength 890 nm	OD ratio
D1	-3.853×10^{-2}	1.565×10^{-3}	–24.610
D2	1.157×10^{-2}	-9.797×10^{-3}	–1.181
D3	-3.678×10^{-2}	2.299×10^{-4}	–1.600
D4	-4.601×10^{-2}	-3.943×10^{-2}	1.167

Referring to Table 5, the first and second columns show the calculated optical density for the first four detectors based on the ray flux values in Table 4. Then, an OD ratio (OD_{735}/OD_{890}) is calculated to represent the ratio, R value corresponds to 70% of fetus oxygen saturation. Among four detectors, only D4 shows the relevant OD ratio since the value of OD ratio is always positive and finite. Extensive analysis needs to be done in order to get a reliable theoretical calibration curve for 735/890 wavelength pair.

6. Conclusions

In real clinical application, the optode array will be handy when measuring the fetus oxygenation transabdominally. As cited in previous literature, the measurement of

fetus signal is much dependent on fetal position with respect to the optode assembly. The fetus in the womb could be in various positions; either near to maternal's abdomen or far away from it. Therefore, it is expected that at least the strongest fetus signal could be captured by any of the detectors that might be at the nearest location with respect to the fetal body without having to use other instruments such as ultrasound imaging to determine the fetus position.

In order to find the best representation of an optode array, a commercial surface--based Monte Carlo algorithm is employed in this study to simulate the effect of optical properties at systolic and diastolic states through the homogenous multilayer tissues of maternal-fetal. The systolic and diastolic optical properties are obtained by calculating the total absorption in tissue using equations as highlighted in the Appendix. A series of simulations have been conducted on two optode array configurations and the results led us to choose the diamond assembly which shows the highest contribution of the ray intensity.

A statistical noise approach is also introduced in this paper in the quest to verify sufficient number of rays to be launched through the system. This step is vital since the accuracy of the results from Monte Carlo simulation also depends on the huge number of rays injected into the system. It is found that 1 million of rays are sufficient enough without a need to sacrifice the amount of time when executing the simulation. In addition, an example of optical density analysis is also described to show the significance of getting the accumulated light intensity at a detector by using systole and diastole properties.

The main finding will be served as a guideline to develop the noninvasive optical probe for fetus oxygenation. Currently, the development of theoretical and empirical calibration which will consider fetus absorption spectrum of hemoglobin is being carried out as well as the development of the instrument before conducting a phantom study.

Appendix

As stated by SCHMITT [33], when tissue is assumed as a homogenous mixture, the total absorption coefficient and total reduced scattering coefficients can be written as:

$$\sum \mu_a = V_a \mu_a^{\text{art}} + V_v \mu_a^{\text{ven}} + \left[1 - (V_a + V_v)\right]\mu_a^t \tag{4}$$

$$\sum \mu_s' = (V_a + V_v)\mu_s^{b'} + \left[1 - (V_a + V_v)\right]\mu_s^{t'} \tag{5}$$

where V_a and V_v are the volume fractions of arterial and venous blood, respectively, with the ratio of 1:3. The total blood volume is $V_0 = 0.0125$ during a diastolic state, whereas 5% increase is detected during a systolic state. The μ_a^{art} and μ_a^{ven} in (4) refer to the absorption coefficient of the arterial and venous blood, respectively, whereas

$\mu_s^{b\prime}$ and $\mu_s^{t\prime}$ in (5) are the reduced scattering coefficients of blood and bloodless tissue, respectively. The $\mu_s^{b\prime}$ and $\mu_s^{t\prime}$ can be calculated using Eq. (3), whereas the μ_a^{art} and μ_a^{ven} are defined as:

$$\mu_a^{\text{art}} = \frac{H}{v_i}\left[S_a O_2 \sigma_a^{100\%} + (1 - S_a O_2)\sigma_a^{0\%}\right] \tag{6}$$

$$\mu_a^{\text{ven}} = \frac{H}{v_i}\left[S_v O_2 \sigma_a^{100\%} + (1 - S_v O_2)\sigma_a^{0\%}\right] \tag{7}$$

where H is hematocrit, whereas v_i is the volume of red blood cells with a typical value for H at 45% and v_i is 90 μm^3, respectively. The $\sigma_a^{100\%}$ and $\sigma_a^{0\%}$ are optical absorption cross-sections of totally HbO_2 and Hb, respectively, and are calculated as [24]:

$$\sigma_a^{100\%} = \frac{v_i}{H\mu_a^{\text{HbO}_2}}, \qquad \sigma_a^{0\%} = \frac{v_i}{H\mu_a^{\text{Hb}}} \tag{8}$$

The arteriovenous difference is assumed to be 10% difference in [33]. Thus, for mother, $S_a O_2$ and $S_v O_2$ are set to be 90% and 80%, respectively, whereas 70% and 60% are the arteriovenous values for fetus.

The total absorption in tissue will be increased during systole due to the increase in the arterial blood, whereas the venous blood is unchanged [24]. To embed this situation, (4) is modified to be:

$$\sum \mu_{a,\,\delta} = V_{a,\,\delta}\mu_a^{\text{art}} + V_v \mu_a^{\text{ven}} + \left[1 - (V_{a,\,\delta} + V_v)\right]\mu_a^t \tag{9}$$

where $\mu_{a,\,\delta}$ and $V_{a,\,\delta}$ are $(\mu_a + \delta_a)$ and $(V_a + \delta V_a)$, respectively. In this case:

$$\delta_a = \delta V_a(\mu_a^{\text{art}} - \mu_a^t) \tag{10}$$

Since, $\mu_a^{\text{art}} \gg \mu_a^t$, hence:

$$\delta_a = \delta V_a \mu_a^{\text{art}} \tag{11}$$

As for the reduced scattering coefficients, [24] and [25] are assumed to be not affected by the small percentage of blood volume in the tissue. Therefore, only $\mu_s^{t\prime}$ part in (5) is used to describe the total reduced scattering coefficient. On the other hand, the absorption coefficient of amniotic fluid, $\mu_{\text{a, af}}$ is assumed to be approximately four times smaller than mother's absorption coefficient, whereas the reduced scattering is assumed to be 0.01 mm^{-1} for all wavelengths [24].

Acknowledgements – This work was supported by a research grant from Universiti Kebangsaan Malaysia (UKM-AP-TKP-07-2009). The authors would like to thanks BRO for licensing the ASAP PRO 2010 to UKM.

References

[1] LILJESTRÖM L., WIKSTRÖM A.-K., HANSON U., AKERUD H., JONSSON M., *Evaluation of the discrepancy between pH and lactate in combined fetal scalp blood sampling*, Acta Obstetricia et Gynecologica Scandinavica **90**(10), 2011, pp. 1088–1093.

[2] CARBONNE B., NGUYEN A., *Fetal scalp blood sampling for pH and lactate managment during labor*, Journal de Gynécologie Obstétrique et Biologie de la Reproduction **37**(1, Supplement), 2008, pp. S65–S71.

[3] MAHENDRU A.A., LEES C.C., *Is intrapartum fetal blood sampling a gold standard diagnostic tool for fetal distress?*, European Journal of Obstetrics and Gynecology and Reproductive Biology **156**(2), 2011, pp. 137-139.

[4] WIBERG-ITZEL E., LIPPONER C., NORMAN M., HERBST A., PREBENSEN D., HANSSON A., BRYNGELSSON A.-L., CHRISTOFFERSSON M., SENNSTRÖM M., WENNERHOLM U.-B., NORDSTRÖM L., *Determination of pH or lactate in fetal scalp blood in management of intrapartum fetal distress: randomised controlled multicentre trial*, BMJ **336**, 2008, p. 1284.

[5] TUFFNELL D., HAW W.L., WILKINSON K., *How long does a fetal scalp blood sample take?*, BJOG: An International Journal of Obstetrics and Gynaecology **113**(3), 2006, pp. 332–334.

[6] WESTGREN M., KRUGER K., EK S., GRUNEVALD C., KUBLICKAS M., NAKA K., WOLFF K., PERSSON B., *Lactate compared with pH analysis at fetal scalp blood sampling: a prospective randomised study*, BJOG: An International Journal of Obstetrics and Gynaecology **105**(1), 1998, pp. 29–33.

[7] MASIN D.I., PAULSEN A.W., BROUILLARD R.G., IYER V.K., *Fetal transmission pulse oximetry*, [In] *Engineering in Medicine and Biology Society, Proceedings of the 19th Annual International Conference of the IEEE*, Vol. 5, 1997, pp. 2326–2329.

[8] RAMANUJAM N., HONG LONG, RODE M., FOROUZAN I., MORGAN M., CHANCE B., *Antepartum, transabdominal near infrared spectroscopy: Feasibility of measuring photon migration through the fetal head in utero*, Journal of Maternal-Fetal Medicine **8**(6), 1999, pp. 275–288.

[9] GRIGNAFFINI A., SONCINI E., RONZONI E., PIAZZA E., ANFUSO S., VADORA E., *Meconium-stained amniotic fluid and fetal oxygen saturation measured by pulse oximetry during labour*, Acta Bio Medica **75**(Suppl. 1), 2004, pp. 45–52.

[10] LINHARTOVA L., KURTANSKY A., SUSKA P., *Correlation between fetal blood oxygen saturation and umbilical blood pH values*, Bratislava Medical Journal – Bratislavske Lekarske Listy **110**(11), 2009, pp. 684–687.

[11] REUSS J.L., *Factors influencing fetal pulse oximetry performance*, Journal of Clinical Monitoring and Computing **18**(1), 2004, pp. 13–24.

[12] MAESEL A., MÅRTENSSON L., GUDMUNDSSON S., MARŠÅL K., *Fetal pulse oximetry: a methadological study*, Acta Obstetricia et Gynecologica Scandinavica **75**(2), 1996, pp. 144–148.

[13] ESZTO M.-L., MOREL O., DEVAL B., THIÉBAUGEORGES O., *Fetal pulse oxymetry*, Gynécologie Obstétrique and Fertilité **35**(6), 2007, pp. 576–581.

[14] RAMANUJAM N., HIELSCHER A.H., RODE M., CHANCE B., FOROUZAN I., VISHNOI G., *Photon migration through fetal head* in utero *using continuous wave, near infrared spectroscopy: clinical and experimental model studies*, Journal of Biomedical Optics **5**(2), 2000, pp. 173–184.

[15] VISHNOI G., HIELSCHER A.H., RAMANUJAM N., CHANCE B., *Photon migration through fetal head* in utero *using continuous wave, near-infrared spectroscopy: development and evaluation of experimental and numerical models*, Journal of Biomedical Optics **5**(2), 2000, pp. 163–172.

[16] ZOURABIAN A., CHANCE B., RODE M., BOAS D.A., RAMANUJAM N., SIEGEL A., *Trans-abdominal monitoring of fetal arterial blood oxygenation using pulse oximetry*, Journal of Biomedical Optics **5**(4), 2000, pp. 391–405.

[17] JACQUES S.L., RAMANUJAM N., VISHNOI G., CHOE R., CHANCE B., *Modeling photon transport in transabdominal fetal oximetry*, Journal of Biomedical Optics **5**(3), 2000, pp. 277–282.

[18] MAWN T., PENGCHENG LI, NIOKA S., CHANCE B., *Transabdominal monitoring of fetal arterial oxygen saturation using pulse oximetry*, [In] *Proceedings of the IEEE 28th Annual Northeast Bioengineering Conference 2002*, 2002, pp. 227–228.

[19] MAWN T., NIOKA S., NIJLAND M., BLOY L., CHANCE B., LEIGH J.S., ELLIOTT M.A., *Effect of errors in baseline optical properties on accuracy of transabdominal near-infrared spectroscopy in fetal sheep brain during hypoxic stress*, Journal of Biomedical Optics **10**(6), 2005, article 064001.

[20] VINTZILEOS A.M., NIOKA S., LAKE M., PENGCHENG LI, QINGMING LUO, CHANCE B., *Transabdominal fetal pulse oximetry with near-infrared spectroscopy*, American Journal of Obstetrics and Gynecology **192**(1), 2005, pp. 129–133.

[21] KOK BENG GAN, ZAHEDI E., ALI M.A.M., *Transabdominal fetal heart rate detection using NIR photopleythysmography: instrumentation and clinical results*, IEEE Transactions on Biomedical Engineering **56**(8), 2009, pp. 2075–2082.

[22] CANPOLAT M., MOURANT J.R., *High-angle scattering events strongly affect light collection in clinically relevant measurement geometries for light transport through tissue*, Physics in Medicine and Biology **45**(5), 2000, pp. 1127–1140.

[23] MUNRO E.A., *Implantable Biosensors for Neural Imaging: A Study of Optical Modeling and Light Sources*, Graduate Department of the Institute of Biomaterials and Biomedical Engineering, University of Toronto, 2009.

[24] GAN K.B., *Noninvasive fetal heart rate detection using nearinfrared and adaptive filtering*, PhD Thesis, Department of Electrical, Electronics and System Engineering, Universiti Kebangsaan Malaysia, Selangor, 2009.

[25] MANNHEIMER P.D., CASCINI J.R., FEIN M.E., NIERLICH S.L., *Wavelength selection for low-saturation pulse oximetry*, IEEE Transactions on Biomedical Engineering **44**(3), 1997, pp. 148–158.

[26] CHAIKEN J., GOODISMAN J., *On probing human fingertips* in vivo *using near-infrared light: model calculations*, Journal of Biomedical Optics **15**(3), 2010, article 037007.

[27] HUEBER D.M., FRANCESCHINI M.A., MA H.Y., ZHANG Q., BALLESTEROS J.R., FANTINI S., WALLACE D., NTZIACHRISTOS V., CHANCE B., *Non-invasive and quantitative near-infrared haemoglobin spectrometry in the piglet brain during hypoxic stress, using a frequency-domain multidistance instrument*, Physics in Medicine and Biology **46**(1), 2001, pp. 41–62.

[28] BEARDEN E.D., WILSON J.D., ZHAROV V.P., LOWERY C.L., *Deep penetration of light into biotissue*, Proceedings of SPIE **4257**, 2001, pp. 417–425.

[29] D. S. Richards, et al. (1992, Umbilical vessels: visualization. Available: http://www.thefetus.net

[30] JACQUES S.L., *Laser tissue interaction*, Cancer Bulletin, 1989, pp. 211–218.

[31] DUBUS I.G., JANSSEN P.H.M., *Issues of replicability in Monte Carlo modeling: a case study with a pesticide leaching model*, Environmental Toxicology and Chemistry **22**(12), 2003, pp. 3081–3087.

[32] WUKITSCH M.W., PETTERSON M.T., TOBLER D.R., POLOGE J.A., *Pulse oximetry: analysis of theory, technology, and practice*, Journal of Clinical Monitoring and Computing **4**(4), 1988, pp. 290–301.

[33] SCHMITT J.M., *Simple photon diffusion analysis of the effects of multiple scattering on pulse oximetry*, IEEE Transactions on Biomedical Engineering **38**(12), 1991, pp. 1194–1203.

Received September 18, 2012